Catal Lett (2008) 124:195–203
DOI 10.1007/s10562-008-9484-7

$La_{1-x}Ca_xNiO_3$ Perovskite Oxides: Characterization and Catalytic Reactivity in Dry Reforming of Methane

S. M. de Lima · M. A. Peña · J. L. G. Fierro · J. M. Assaf

Received: 21 December 2007 / Accepted: 3 April 2008 / Published online: 24 April 2008

Abstract Perovskite-type oxides such as $La_{1-x}Ca_xNiO_3$ ($x = 0.0$, 0.05, 0.1, 0.3, 0.5 and 0.8) have been prepared from citrate precursors and characterized by XRD, TPR, TG-H_2 and XPS. Catalytic experiments in the reforming of CH_4 with CO_2 have been carried out in a tubular reactor at 750 °C and atmospheric pressure. After the catalytic tests the catalysts were studied by TPO and SEM. Partial substitution of La by Ca was performed to stabilize Ni particles and to prevent carbon deposition. The XRD profiles showed that the perovskite structure is the only compound identified within the $0 \leq x \leq 0.05$ range, whereas for $x \geq 0.1$ compounds such as spinel-type La_2NiO_4, NiO and CaO were observed in addition to the perovskite oxide. On the other hand, segregation of NiO, even in the unsubstituted perovskite ($x = 0.0$), was confirmed by TPR and XPS. The catalytic tests showed that the replacement of La by Ca, which has a lower ionic radius, favored a higher activity and stronger resistance to carbon deposition. However, this coking resistance depended on the Ca-loading and the catalysts with $x = 0.05$ and $x = 0.8$ were the most stable against deactivation.

Keywords CO_2 reforming of methane · La–Ca perovskites · Syngas · Redox properties

S. M. de Lima (✉) · J. M. Assaf
Departamento de Engenharia Química, Universidade Federal de São Carlos, Laboratório de Catálise, Sao Carlos CEP 13565-905, Brazil
e-mail: psania@iris.ufscar.br

M. A. Peña · J. L. G. Fierro
Instituto de Catálisis y Petroleoquímica, CSIC, Cantoblanco 28049, Madrid, Spain

1 Introduction

New reserves of natural gas have been identified and potentially represent a new source of raw material for industry, being able, in many cases, to substitute the petroleum that has been steadily rising in price and whose rate of production is expected to fall in the near future. Methane is the main component of natural gas and one of the ways by which it can be used involves initially converting it to synthesis gas ($CO + H_2$), which is subsequently transformed into valuable products that are easier to transport. Synthesis gas can be used in the production of liquid hydrocarbon fuels by the Fischer–Tropsch synthesis or in methanol production [1]. In these processes, the production of synthesis gas is considered to account for around 60%–70% of the total capital cost [2, 3]. Thus, their economic viability relies strongly on reducing the costs of synthesis gas generation and alternative routes to syngas production should be considered. The process of carbon dioxide reforming of methane has been extensively studied and also has important environmental implications because CH_4 and CO_2 emissions in the atmosphere lead to global warming through the greenhouse effect and both gases can be simultaneously converted to synthesis gas.

$$CH_4 + CO_2 \rightarrow 2CO + 2H_2 \quad (1)$$

In addition, this process allows the production of syngas with a H_2/CO ratio more convenient for further applications: while higher H_2/CO ratio favors methane and inhibits chain growth [4–6]; a low H_2/CO ratio favors the methanol to gasoline process for ethane, propane and aromatics from methanol [7]. Alkenes, oxygenates, hydroformylation and acetic acid production are also favored at low H_2/CO ratios [8–11].

It is well known that noble metals such as Rh, Ru or Pt and transition metals, mainly Ni and Co, show high

catalytic activity for the reforming reaction. Though noble metal catalysts are less sensitive to carbon deposition [12, 13], supported Ni catalyst is often used because of the big difference in price [14, 15]. The main problem that prevents this process from being used industrially is that supported Ni catalysts are easily deactivated by carbon deposition. It has been reported that the carbon formation can be suppressed by the addition of oxides of alkaline or alkaline-earth metals with high basicity and of lanthanides [16], or by the use of highly dispersed metal species [17] on the support, thus increasing the catalytic stability. A particularly attractive option is the use of mixed metal oxide precursors with perovskite structure, which also display an exceptionally high thermal stability. The general formula of these oxides is ABO_3, in which the cation A is responsible for the thermal resistance of the catalyst whereas the cation B is responsible for the catalytic performance. The perovskites do not only fulfill the stability requirements, but also by further reduction of B-site cations which remain distributed in the structure, they result in the formation of a well-dispersed and stable metal particle catalysts [18].

Studies on $LaCoO_3$ [19] and $LaNiO_3$ [20] perovskites indicate that, by reduction treatment, the metal (Co, Ni) is in a highly disperse state on a matrix composed of the respective metal oxide. Although many previous investigations of the CO_2 reforming of methane have been carried out over transition metals supported on alumina, silica and magnesia [21–26], the use of perovskite-type oxides has been less studied [27–32].

Since the properties of the precursor perovskite can be modified, according to the choice and stoichiometry of A- and B-site cations, it was decided to investigate the effects of such changes. Thus this article was undertaken with the aim to examine the influence of the addition of Ca to the $LaNiO_3$ structure to form the $La_{1-x}Ca_xNiO_3$ structure ($x = 0.0$, 0.05, 0.1, 0.3, 0.5 and 0.8), on the properties and catalytic performance in the CO_2 reforming of methane, so as to prevent carbon formation. Calcium as A-site cation was selected taking into account its basic character, which should further inhibit coke formation.

2 Experimental

2.1 Catalysts Preparation

The perovskite-type oxides $La_{1-x}Ca_xNiO_3$ were synthesized by a modification of the citrate method [31]. A concentrated solution of citric acid (p.a., from Merck) was prepared and added to a solution of the precursor of the B-site cation ($Ni(NO_3)_2 \cdot 6H_2O$ (Aldrich)) with an excess of ethylene glycol, and the mixture was kept at 60 °C for 1 h under constant stirring. Then, solutions of lanthanum and calcium nitrates (Aldrich) were added, the whole remaining at 60 °C for 1 h more. The resulting solution was slowly evaporated at 110 °C for 48 h until a spongy material was obtained. This citrate precursor was crushed and decomposed at 550 °C for 3 h and finally calcined at 900 °C for 10 h to obtain the final mixed oxide.

2.2 Characterization Techniques

X-ray diffraction (XRD) patterns of all calcined samples were obtained in a Siemens D-5005 diffractometer with CuK_α radiation in the 2θ scanning mode (range 5–80°). For crystal phase detection, the patterns recorded were referred to the powder diffraction files of the JCPDF database cards.

Temperature-programmed reduction (TPR) experiments were carried out on a semiautomatic Micromeritics TPD/TPR 2900 apparatus interfaced with a microcomputer. Samples of about 30 mg were placed in a U-shaped quartz tube initially purged in a synthetic air stream of 50 mL/min at 500 °C for 1 h and then cooled to room temperature. Reduction profiles were then recorded by passing a stream of 10% H_2/Ar at a flow rate of 50 mL/min, while heating the sample at a rate of 10 °C/min from ambient temperature to 900 °C. Under these conditions, the parameter $P = \beta \cdot S_o/F \cdot C_o$, where β is the heating rate, S_o is the amount of reducible Ni^{3+} species in the sample, and $F \cdot C_o$ is the hydrogen feed in the reactor, reaches a value of 10.9 K, which is within the range where line profile and peak positions can be accurately measured (see, e.g., [33]). A cold-trap was placed just before the thermal conductivity detector (TCD) of the instrument to remove the water from the exit stream. After each step of reduction of the sample with $x = 0.3$, it was passivated with a 1% O_2/He mixture and XRD patterns were recorded to support a more accurate identification of one of the reduction peaks.

The reducibility of the samples was also evaluated by thermogravimetry in a hydrogen atmosphere (TG-H_2), by recording the weight loss on a Mettler Toledo TGA/SDTA851 microbalance. The weight change of each sample (ca. 30 mg) was recorded while heating at a rate of 10 °C/min up to 1,000 °C in a stream of 50 mL/min of 10% H_2/N_2 gas mixture.

X-ray photoelectron spectra (XPS) were acquired with a VG Escalab 200R spectrometer equipped with a hemispherical electron analyzer and a Mg K_α ($h \cdot \nu = 1253.6$ eV) X-ray source. The powder samples were pressed into small Inox cylinders and then mounted on a sample rod placed in a pretreatment chamber of the spectrometer. The background pressure in the analysis chamber was kept below $1 \cdot 10^{-8}$ mbar during data acquisition. The XPS data were signal-averaged over at least 300 scans and were taken in increments of 0.1 eV, with dwell times of 50 ms, and an electron analyzer pass energy of 50 eV. Peak intensities were

estimated by integrating the area under each peak after smoothing and subtraction of Shirley background and fitting of the experimental peak by a least-squares routine to Gaussian and Lorentzian curves. Atomic ratios were computed from the peak intensity ratios normalized by atomic sensitivity factors [34]. The binding energy (BE) reference was taken as the C 1s peak from carbon contamination of the samples at 284.9 eV.

Temperature-programmed oxidation (TPO) was performed on catalysts after the catalytic tests in a TA Instruments SDT 2960 Simultaneous TGA analyzer, at a heating rate of 10 °C/min, from room temperature up to 900 °C in an oxidizing atmosphere, to verify possible carbon formation. The morphology of the carbon deposits was examined in a Zeiss DSM 940A scanning electron microscope.

2.3 Catalytic Activity Measurements

The catalytic reforming reaction of methane with carbon dioxide was carried out in a fixed-bed quartz tubular reactor (i.d. 10 mm) under atmospheric pressure. The reactant gases CH_4/CO_2 were in a molar ratio of 1:1, and a total gas flow rate of 120 mL/min. The samples of catalyst (100 mg) were first reduced in situ for 5 h at 700 °C in a flow of pure hydrogen (40 mL/min) and then tested at 750 °C for approximately 10 h. The reactants and products were analyzed by on-line Varian GC-3800 gas chromatograph provided with two thermal conductivity detectors and columns packed with Porapak N and 13X molecular sieves. The conversions of CH_4 and CO_2 were defined as the converted CH_4 and CO_2 per total amount of CH_4 and CO_2 in the reactor feed, respectively.

3 Results and Discussion

3.1 Catalysts Characterization

The X-ray diffraction profiles (Fig. 1) of the calcined samples ($x = 0.0$ and 0.05) revealed that the conditions used during calcination were sufficient to produce the perovskite structure as the main phase present. However, in the catalysts with $x \geq 0.1$, there are also reflection lines for NiO and an additional spinel-type phase of La_2NiO_4, of intensity increasing with x. At values of $x \geq 0.3$, besides these detected phases, diffraction lines for CaO are seen. An important observation is that at high contents of Ca the dominant phases are NiO and CaO, but reflections for the spinel and perovskite phases still exist.

Since the active sites for the reforming reaction are metallic nickel crystallites, the oxide precursors must be activated in a reducing atmosphere prior to reaction. In this way, a highly dispersed supported Ni metal catalyst on a matrix of La–Ca–O is obtained. In order to study this activation process, the reducibility of $La_{1-x}Ca_xNiO_3$ systems was examined by temperature-programmed reduction and the reduction profiles being displayed in Fig. 2. To confirm the observations and to identify some reduction step that was not very clear in TPR analysis, thermogravimetry in a hydrogen atmosphere (TG-H_2) was also performed (Fig. 3).

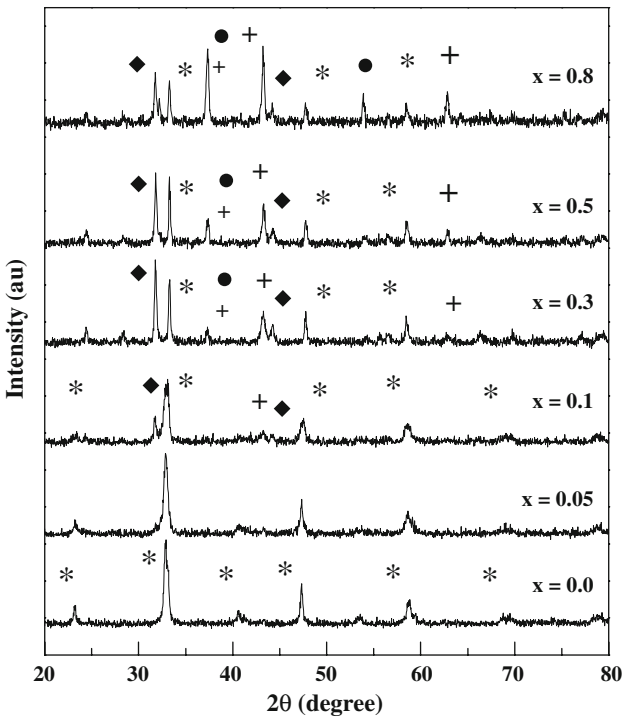

Fig. 1 X-ray diffraction (XRD) patterns of $La_{1-x}Ca_xNiO_3$ perovskite oxides calcined at 900 °C. $LaNiO_3$ perovskite (*), CaO (•), NiO (+) and La_2NiO_4 (♦)

The $LaNiO_3$ perovskite ($x = 0.0$) exhibited two reduction steps: the first due to the formation of $La_2Ni_2O_5$, representing the reduction of Ni^{3+} to Ni^{2+} (350 °C), and the second associated with reduction of Ni^{2+} to Ni^0 that remains supported on lanthanum oxide (495 °C) [30]. The ratio of the areas under the first and second peaks is 1:2, corresponding to the expected hydrogen consumption for both processes

When La is partially substituted by Ca, the first peak shifts to higher temperature (ca. 380 °C), with small variations in the position peak for the different Ca-doped catalysts. For $x = 0.05$, there is a shoulder at ca. 350 °C, whose intensity decreases for $x = 0.1$ and disappear for greater values of x. Besides, the second peak also shifts at higher temperature for $x = 0.05$ (510 °C) and $x = 0.1$ (520 °C). This behavior could be initially understood as a lower reducibility of the Ca-substituted perovskite. Nevertheless, it should be noted that the ratio of intensity

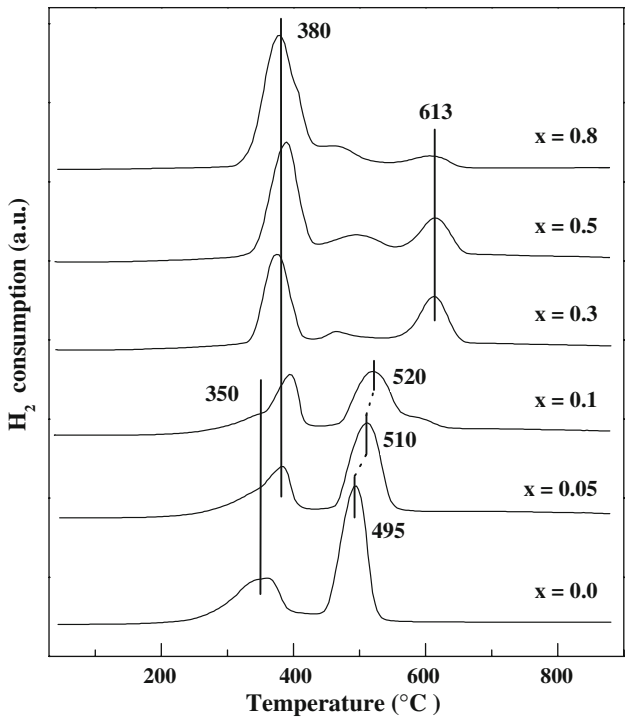

Fig. 2 TPR profiles of different $La_{1-x}Ca_xNiO_3$ catalysts calcined in air at 900 °C

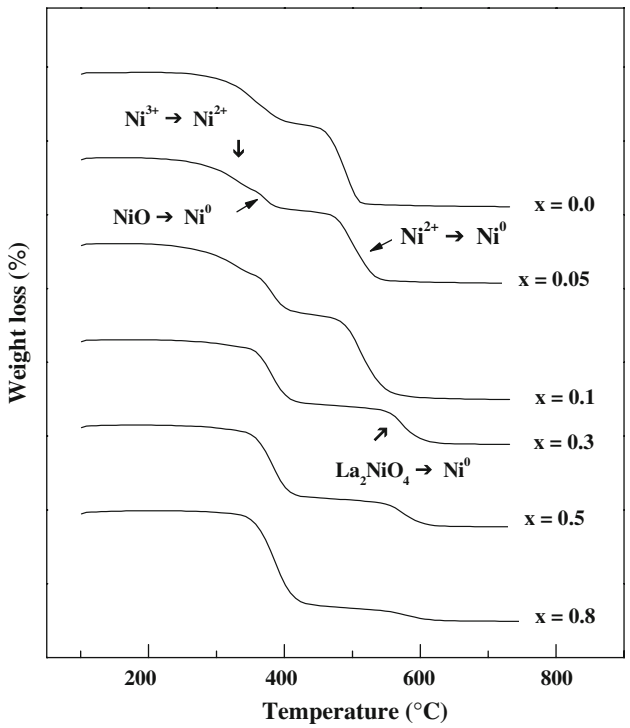

Fig. 3 Weight losses as a function of temperature of $La_{1-x}Ca_xNiO_3$ catalysts heated in a hydrogen flow

between the first and second peaks is not 1:2 as it should be expected in the reduction of the perovskite, and that NiO was detected as a segregate phase in the Ca-containing samples in the XRD patterns together with the perovskite structure (Fig. 1). Therefore, it can be concluded that, for the hydrogen consumption of the first peak at 380 °C, there is a contribution of the reduction of Ni^{2+} to Ni^0 in the NiO phase, which happen almost simultaneously with the first step of reduction of the perovskite. This contribution is detected even for $x = 0.05$, where no NiO was detected by XRD (Fig. 1). It is also possible to note an increase in intensity of this peak with increasing Ca content, in other words, with a larger amount of NiO phase detected on XRD.

Similar results were obtained by García de la Cruz et al. [35] who, in a study of $La_{1-x}Sr_xNiO_3$ perovskites, observed the formation of segregated Ni and Sr oxides at $x \geq 0.05$, besides the perovskite phase. They noted in TPR curves that the first reduction peak splits into two at $x \geq 0.02$, the intensity of the second rising with x, and associated the latter peak with reduction of a small amount of segregated NiO, despite its not being identified by XRD. The existence of this phase was supported by the results of XPS analysis, which showed a significant proportion of Ni^{2+} ions among the Ni^{3+} ions at the surface of the catalyst.

The TG-H_2 curves (Fig. 3) also show the different steps in reduction detected by TPR. By measuring the mass lost in the three reduction steps and knowing that, for the perovskite structure, the loss due to reduction of Ni^{3+} to Ni^{2+} should be half that due to reduction of Ni^{2+} to Ni^0, the result obtained from the TPR analysis can be confirmed, namely that the intermediate reduction step is related to reduction of NiO.

The behavior of the second peak a higher temperature changes for $x \geq 0.3$. The peak shifts abruptly to 610 °C, and a small peak appears at ca. 480 °C–500 °C (Fig. 2). Requies et al. [36] studied Ni/La_2O_3 catalysts with 10%, 20% and 30% Ni, calcined at 1,000 °C, and observed both the perovskite structure ($LaNiO_3$) and a spinel phase of the type La_2NiO_4 in all the samples. However, the lower the Ni content, the greater was the proportion of the spinel phase and the smaller that of the perovskite structure. In TPR profiles, those authors also observed three peaks; they provisionally assigned the first two to the reduction of nickel in the perovskite structure to Ni^0 and the third, seen at about 622 °C, to the reduction of nickel in the spinel phase. This was confirmed by comparing the TPR profiles of the three samples; when the Ni content dropped to 10%, there was a drastic fall in the intensity of the first two reduction peaks and a marked rise in that of the third, showing that the third peak could only be assigned to the reduction of Ni in the spinel, as this was the predominant phase in this sample.

In the present study, XRD results show clear presence of the La_2NiO_4 spinel phase for $x \geq 0.3$, and, analogously to the case described by Requies et al. cited above, this peak

at 610 °C can be assigned to the reduction of nickel in this phase. For the higher value of x (0.8) the main crystalline phase in the XRD pattern is NiO, explaining that the main reduction peak in the TPR profile for this catalysts were at 380 °C. The appearance of an additional peak at ca. 480 °C–500 °C could indicate that a small part of the NiO segregated crystallites interact distinctly with the surrounding particles (mainly the spinel phase), producing Ni^{2+} sites that are slightly more difficult to reduce.

To verify that this TPR peak really refers to reduction of the spinel phase, XRD patterns were recorded after each step in the reduction of the sample with $x = 0.3$ and these are displayed in Fig. 4. Proceeding through successive stages of reduction, we observe that the lines assigned to both the perovskite structure and the spinel phase decline, but continue to be present in the first two reduction steps. Only after the third and final step does La_2O_3 appear, as all the Ni is reduced to metal, confirming the hypothesis regarding the TPR results.

The chemical state of the elements and surface composition of the $La_{1-x}Ca_xNiO_3$ mixed oxides were revealed by photoelectron spectroscopy. Although this surface characterization has been carried out on the oxide before the activation of the perovskite by reduction in hydrogen, was found that it is possible to find a good correlation between the results described here and the catalytic activity of the metal supported catalyst formed during this activation process. The binding energies of O 1s, C 1s, Ni $2p_{1/2}$, La $3d_{5/2}$ and Ca 2p core-levels of calcined $La_{1-x}Ca_xNiO_3$ samples, are summarized in Table 1. In addition, with the aim to show spectral features, the corresponding spectra are displayed in Fig. 5.

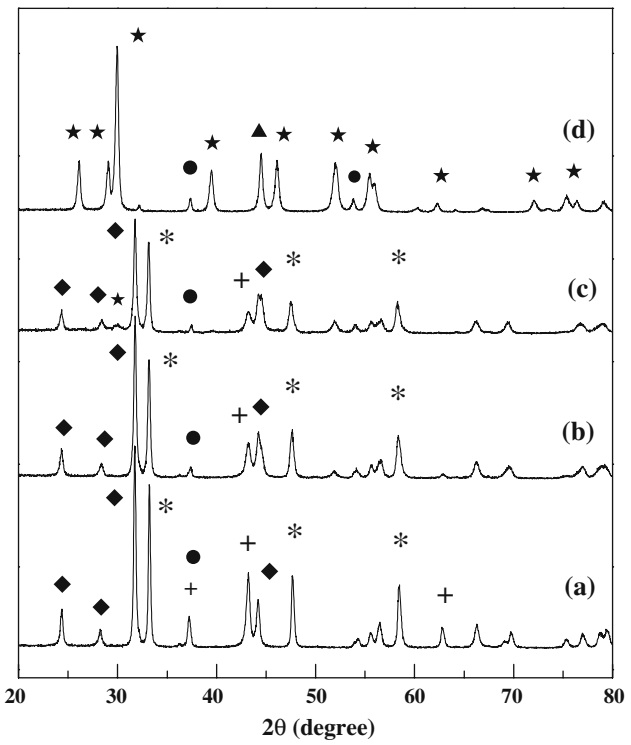

Fig. 4 X-ray diffraction (XRD) patterns of $La_{1-x}Ca_xNiO_3$ perovskite oxide with $x = 0.3$; (**a**) before reduction; (**b**) reduced at 420 °C; (**c**) reduced at 550 °C and (**d**) reduced at 700 °C. $LaNiO_3$ perovskite (*), CaO (•), NiO (+), La_2NiO_4 (♦),La_2O_3 (★) and Ni^0 (▲)

These data show that the binding energy of La $3d_{5/2}$ remains constant when the La^{3+} is replaced by Ca^{2+} in the perovskite structure. Also, three photoemission lines can be seen for O 1s, which correspond to three distinct oxygen species [37] that are present in all the samples. The line with lowest binding energy (528.9–529.1 eV) is attributed to oxygen ions in the crystal lattice (O^{2-}), the intermediate energy line (530.8–531.1 eV) to oxygen in hydroxyl and/or carbonate groups and that with highest binding energy (532.0–532.4 eV) to strongly adsorbed molecular water [19].

The Ni 2p profiles are very complex because of the overlapping of Ni $2p_{3/2}$ and La $3d_{3/2}$ peaks (Fig. 5). Owing to the proximity of the binding energies of Ni^{2+} and Ni^{3+}, it is difficult to distinguish each of these species. The most intense peak for Ni $2p_{3/2}$, which appears around 855 eV, is typical of Ni^{2+}/Ni^{3+} ions surrounded by oxide ions [38]. This peak is accompanied by a satellite line, positioned about 6 eV to the high binding-energy side of the peak (ca. 861 eV), which constitutes a "fingerprint" of Ni^{2+} ions and provides conclusive evidence of their presence in significant numbers at the sample surface, together with the Ni^{3+} ions. These results agree with the XRD data that indicated the presence of NiO and La_2NiO_4, in both of which the Ni occurs as the divalent cation.

Table 1 Binding energies (eV) of core levels of $La_{1-x}Ca_xNiO_3$ samples (figures in parenthesis indicate intensity percentage of O 1s components)

Sample	$Ca2p_{3/2}$	La $3d_{5/2}$	Ni $2p_{1/2}$	O 1s
$x = 0.05$	347.2	834.3	872.8	528.9 (32)
				530.9 (35)
				532.0 (33)
$x = 0.1$	347.0	834.4	872.9	529.1 (31)
				531.1 (42)
				532.4 (27)
$x = 0.3$	346.9	834.4	872.8	528.9 (28)
				530.9 (49)
				532.3 (23)
$x = 0.5$	346.9	834.3	872.7	528.9 (34)
				530.8 (44)
				532.2 (22)
$x = 0.8$	347.0	834.3	872.7	529.0 (30)
				530.8 (47)
				532.0 (23)

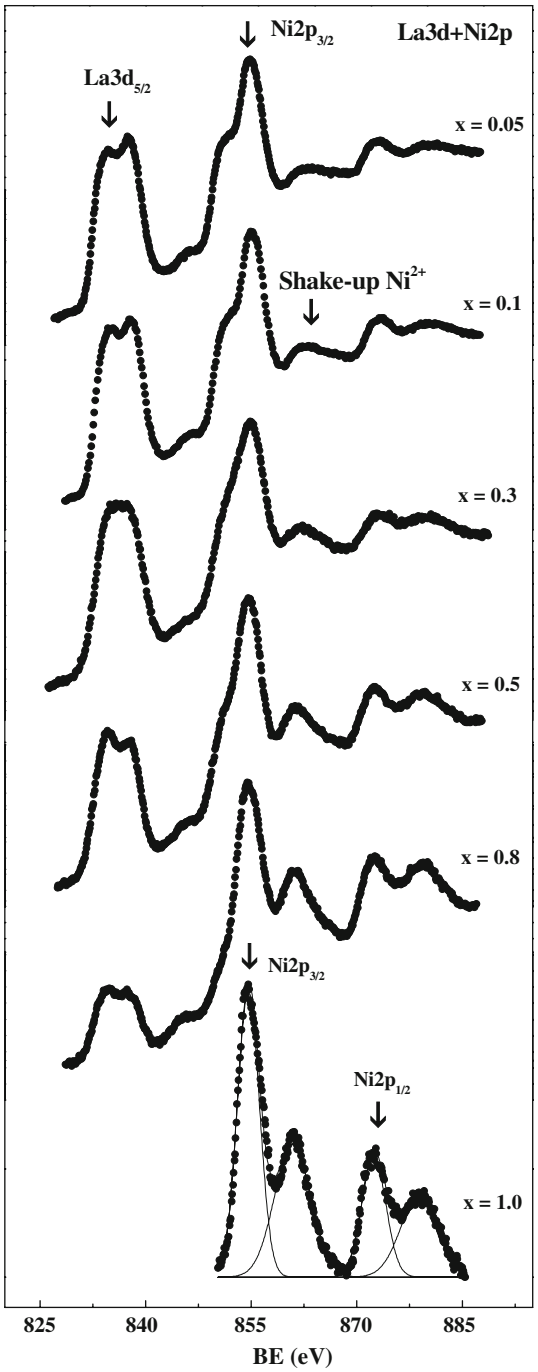

Fig. 5 La3d + Ni2p core-level spectrums of $La_{1-x}Ca_xNiO_3$ catalysts calcined in air at 900 °C

To avoid the region where the most intense Ni 2p line (Ni $2p_{3/2}$) overlaps the less intense line in the La 3d doublet (La $3d_{3/2}$), the region of the Ni $2p_{1/2}$ peak (near 872.4 eV) and its satellite line (near 879.0 eV) was used for quantitative estimates of energy and intensity. Analogously, the energy region of the La $3d_{5/2}$ emission was chosen for careful measurement of the position of the most intense peak.

The surface atomic ratios (Fig. 6) were calculated from the peak intensities and theoretical atomic sensitivity factors determined by Wagner et al. [39]. In Fig. 6, the experimental XPS atomic ratio is compared with the bulk composition of the substituted perovskite. Ni/La atomic ratio indicates an enrichment of nickel in the surface of the samples, indicating that NiO phase found by XRD and TPR is segregated mainly to the surface. It is very interesting the progression of the Ca/Ni surface ratios. It can be observed a great enrichment of calcium in the surface of the samples for $x = 0.05$ and $x = 0.1$, indicating that most of the incorporated calcium remains in the surface. For higher values of x, the surface Ca concentration is the expected for the bulk composition. This could be connected with the tendency of alkaline-earth ions to react with atmospheric CO_2, producing surface carbonates. As a matter of fact, the ratio $CO_3^{2-}/(La + Ca)$ is in the range 0.6–1.0 for the different catalysts.

3.2 Catalyst Activity

The results of the catalytic activity tests, in terms of conversion of CH_4 and CO_2 to products, showed that all the

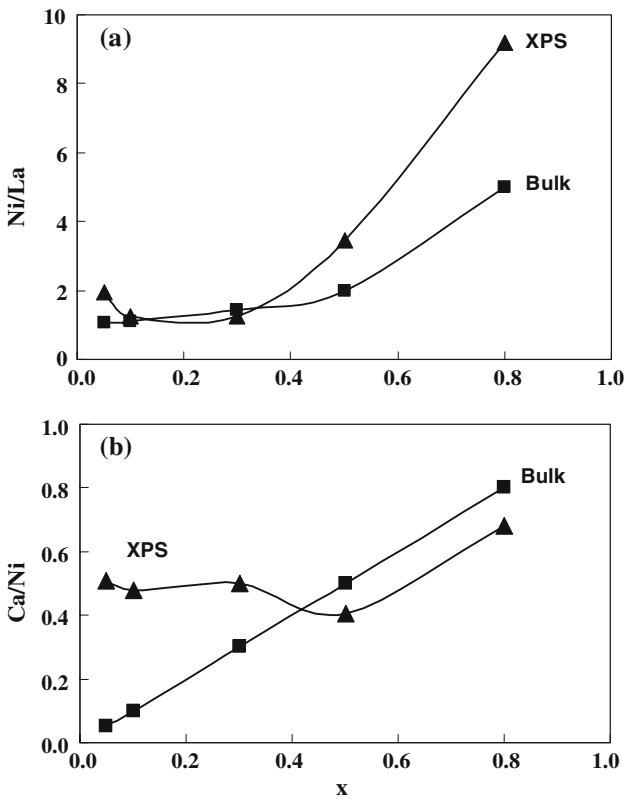

Fig. 6 Ni/La (**a**) and Ca/Ni (**b**) surface atomic ratios measured by XPS compared with the calculated atomic ratios for the bulk composition

catalysts were active for the dry reforming of methane (Figs. 7 and 8).

For most of the catalysts, the conversion of CH_4 and CO_2 began to rise during the reaction time, tending to reach a steady state. Only in the unsubstituted sample ($LaNiO_3$), and in sample with $x = 0.3$, a small decrease of methane conversion with the time on stream was detected. This gradual loss of activity is probably caused by the accumulation of carbon formed as a byproduct on the surface. It was also noted that the CO_2 conversion was always greater than that of CH_4. This happens because the reverse water gas shift reaction (Eq. 2), which also consumes CO_2, occurs in parallel with the dry reforming of methane, keeping the H_2/CO product ratio below unity (Fig. 9).

$$CO_2 + H_2 \rightarrow CO + H_2O \quad (2)$$

Rynkowski et al. [40], investigating the catalysis of dry reforming of methane by $La_{2-x}Sr_xNiO_4$ oxides, observed that the Sr-free sample suffered deactivation during 24 h of reaction at 900 °C, due to the carbon deposited on the catalytic surface, whereas samples containing Sr ($x = 0.25$ and 0.5) remained stable throughout the reaction, despite exhibiting small amounts of deposited carbon. They further reported that at high Sr contents ($x > 0.75$) the catalysts were completely free from carbon deposits, but had very little catalytic activity. The authors attributed this low activity to the formation of a layer of $SrCO_3$ over the active Ni species at the surface and concluded that increasing the amount of strontium raised the basicity of the catalyst surface, thus increasing its capacity to chemisorb CO_2. The higher concentration of adsorbed CO_2 would tend to decrease the formation of free carbon (coking) by the disproportionation of CO. The authors hypothesized that low Sr contents altered the geometric nature of the catalyst

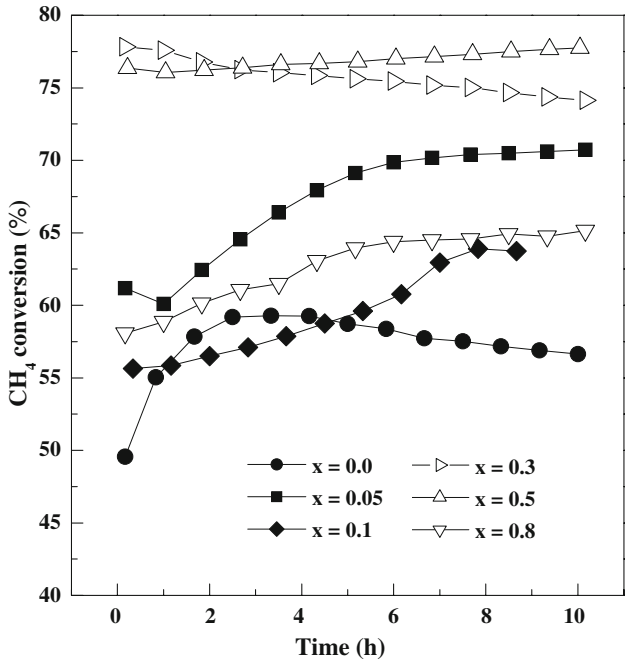

Fig. 7 Catalytic activity (CH_4) as a function of the reaction time for $La_{1-x}Ca_xNiO_3$ perovskites at 750 °C. Flow rate = 120 mL/min; catalyst weight = 0.10 g

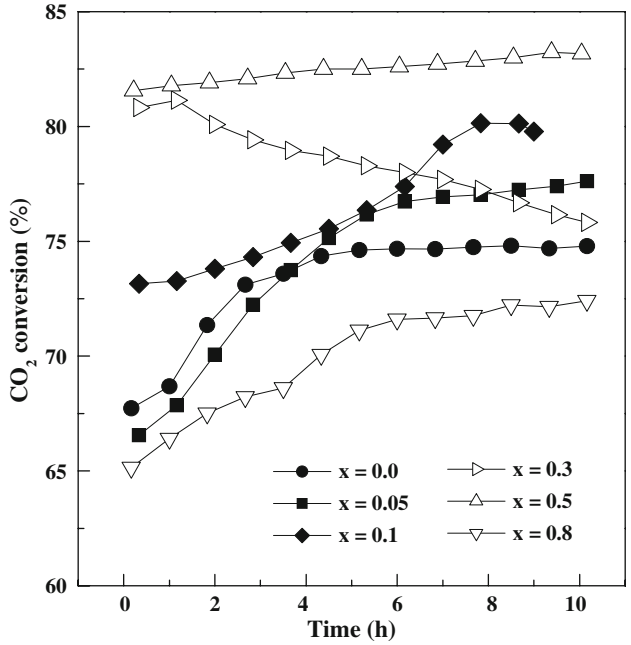

Fig. 8 Catalytic activity (CO_2) as a function of the reaction time for $La_{1-x}Ca_xNiO_3$ perovskites at 750 °C. Flow rate = 120 mL/min; catalyst weight = 0.10 g

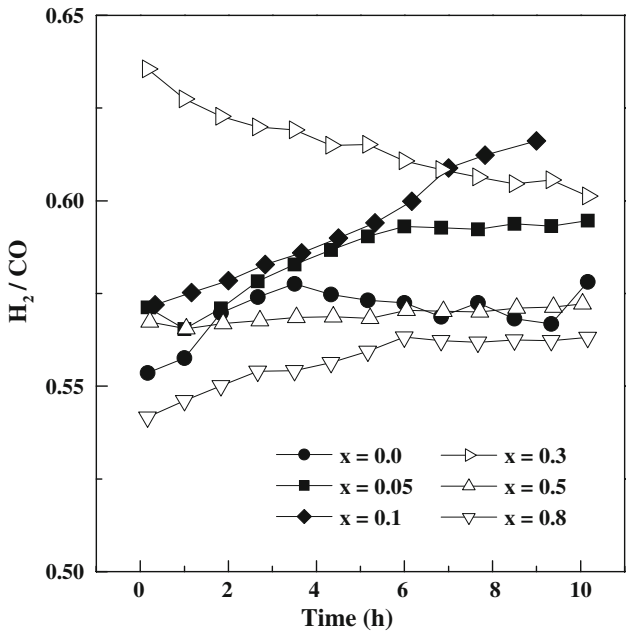

Fig. 9 H_2/CO ratio as a function of the reaction time for $La_{1-x}Ca_xNiO_3$ perovskites at 750 °C. Flow rate = 120 mL/min; catalyst weight = 0.10 g

surface, i.e., dividing the nickel particles into smaller ensembles less prone to coking.

The role of calcium substitution in the nickel perovskite could be similar, but it has been evidenced here in a different way. First of all, deactivation has been only observed, and in low extension, for the Ca-free perovskite and for the intermediate composition $La_{0.7}Ca_{0.3}NiO_3$. Additionally, most of the systems display an increase of methane conversion with the time of reaction. This change in activity when the samples are in the presence of the reactive mixture indicates a change in the nature of the active sites (metallic nickel particles), implying that during reaction, the interaction of this Ni crystallites with the support phase (lanthanum and calcium oxides) is modified. Moreover, the deactivation produced by carbon deposits was not observed for most of the catalyst, and it can be only detected in the two samples commented above. Figure 10 shows the quantification of the carbon deposited in the surface of the catalysts, measured by TPO. Although the two catalysts where deactivation was found ($x = 0.0$, 0.3) exhibit high amount of surface carbon, similar amount of coke is found in catalysts with good stability. It thus seems that the carbon deposits detected by TPO were not mainly of the encapsulated type, which would coat the metal surface and cause a loss of activity [41]. During the initial hours of reaction, the activation of the metallic nickel sites seems to be more important, for most of the catalysts, than the deactivation by the fraction of encapsulated carbon that is deposited on the surface, producing an increasing of the conversion.

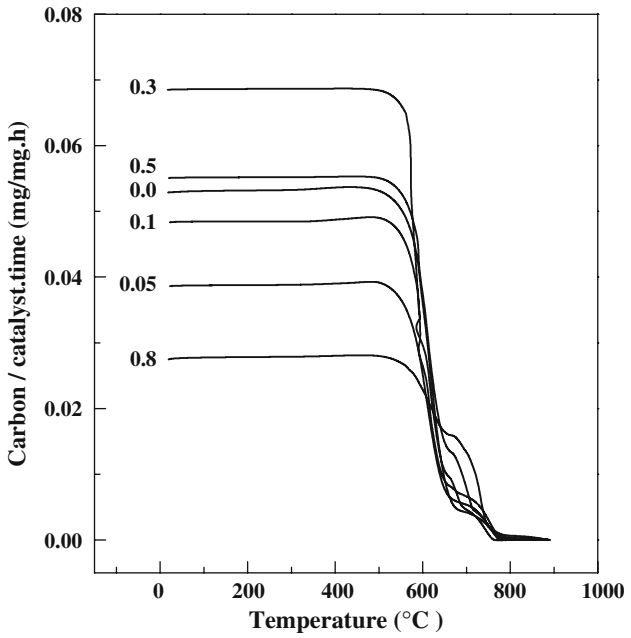

Fig. 10 Temperature-programmed oxidation curves of the $La_{1-x}Ca_xNiO_3$ catalysts after the stability test

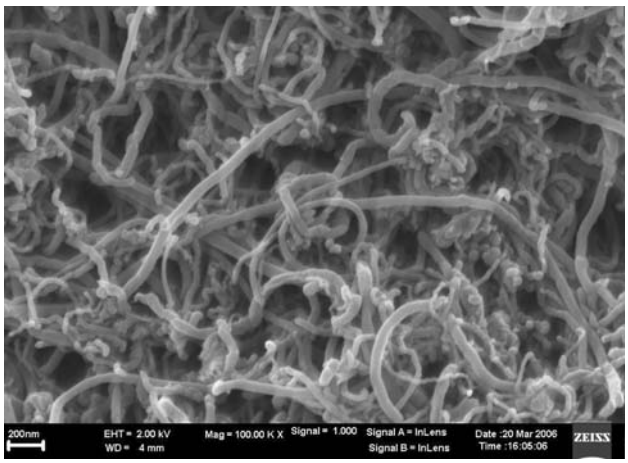

Fig. 11 SEM micrographs of the $La_{0.5}Ca_{0.5}NiO_3$ catalyst after the stability test

In scanning electron microscope (SEM) images (Fig. 11), it was observed on all the catalysts that the carbon was deposited in the form of filaments, which are characteristic of methane-reforming reactions. For this deposition to occur, methane must first dissociate at the surface, producing adsorbed atomic carbon, denominated C_α. This phase is highly reactive and an essential part of the mechanism of reforming reactions, in which it has to be removed from the catalytic surface by adsorbed atomic oxygen that originates from the oxygenated reagent [42]. If there is a shortage of this atomic oxygen, this removal may not occur immediately, allowing carbon atoms to dissolve in the nickel surface and diffuse across the metal to its interface with the oxide support, where they form a phase of carbon fibers or "*whiskers*" [43]. From the start, these fibers do not affect the activity of the nickel, as the curves in Fig. 7 show, because the carbon accumulates between the nickel and support, leaving the metal particle accessible to the reagents. Nevertheless, the volume of the packed catalytic bed tends to rise, producing an increase in the pressure-drop across the catalyst [43].

The methane and CO_2 conversion are in general higher for catalysts containing Ca. The maximum values of conversion are reached for $x = 0.3$ and 0.5 (although with catalytic deactivation for the first one). There is not a direct correlation of activity with the nickel surface concentration, and the segregation of NiO has not an apparent influence either, since the preferential presence of this phase in the surface increases with x (see Fig. 6a). More interesting is the variation of surface segregated calcium (Fig. 6b) when is compared with the catalytic activity. The addition of Ca to the perovskite structure increases the activity, but just in a limited extension for $x = 0.05$ and 0.1. For these two compositions, there is a very high segregation of Ca to the surface (Fig. 6b), hindering partially

the promotion effect in these catalysts. Besides, these catalysts display an important evolution during the time on stream, increasing the conversion by modification of the interaction of the active sites with the support, as has been previously described, but with a relatively low formation of surface coke (Fig. 10). The composition is optimized for $x = 0.3$ and 0.5, with the presence of the doping Ca but a reduced surface segregation (Fig. 6b). Increasing of the Ca content ($x = 0.8$) reduces the carbon deposition (Fig. 10), but producing a less active catalysts (Figs. 7 and 8).

4 Conclusions

According to the XRD patterns obtained, the $La_{1-x}Ca_xNiO_3$ oxides exhibited a single phase with a perovskite structure, in samples with $0.0 \leq x \leq 0.05$, while a mixture of this structure with La_2NiO_4, NiO and CaO phases was detected at $x \geq 0.1$. Nonetheless, when the samples were analyzed by TPR, TG-H_2 and XPS, the NiO phase was observed together with the perovskite structure, even at $x = 0.05$. The partial replacement of La by Ca usually led to increased catalytic activity and better resistance to carbon formation, but this resistance also depended on the actual Ca content. Thus, although the catalysts with x-values of 0.3 and 0.5 were found to be the most actives, they also exhibited the highest amounts of deposited carbon. The segregation of Ca to the surface for different values of x can explain the values of methane and CO_2 conversion, with a appropriate balance of the promotion effect of the La substitution, and a high Ca surface concentration that hindering this promotion effect.

Acknowledgments The authors are grateful to the Ministry of Science and Technology in Spain (Project MAT2001-2215-C03-01) and to FAPESP and CNPq in Brazil for funding this work.

References

1. Bharadwaj SS, Schmidt LD (1995) Fuel Process Technol 42:109–127
2. Lakhapate PJ, Prabhu VK (2000) Chem Eng World 35:77
3. Oil Gas J. 15 (June) (1998) 34.
4. Iglesias E (1997) Appl Catal A: Gen 161:59
5. Bjorgen M, Kolboe S (2002) Appl Catal A: Gen 225:285
6. Rostrup-Nielsen JR (1994) Stud Surf Sci Catal 81:25
7. Kitchen D, Pinto A (1991) Ammonia Plant Saf Relat Facil 31:219
8. Dry ME (2002) Catal Today 71:227
9. Rostrup-Nielsen JR (2002) Catal Today 71:243
10. Cubeiro ML, Morales H, Goldwasser MR, Pérez-Zurita MJ, González-Jiménez F (2000) React Kinet Catal Lett 69:259
11. Guczi L, Koppány Zs, Sarma KV, Borkó L, Kiricsi I (1997) Stud Surf Sci Catal 105:861
12. Rostrup-Nielsen JR, Bak Hansen JH (1993) J Catal 144:38
13. Au C-T, Ng C-F, Liao M-S (1999) J Catal 185:12
14. Wang S, Lu GQ (1998) Appl Catal A: Gen 169:271
15. Ito M, Tagawa T, Goto S (1999) Appl Catal A: Gen 177:15
16. Cao L, Chen Y, Li W (1997) Stud Surf Sci Catal 107:467
17. Bartholomew CH (1982) Catal Rev-Sci Eng 24:67
18. Goldwasser MR, Rivas ME, Pietri E, Pérez-Zurita MJ, Cubeiro ML, Gingembre L, Leclercq L, Leclercq G (2003) Appl Catal A: Gen 255:45–57
19. Crespin M, Hall WK (1981) J Catal 69:359
20. Choudary VR, Uphade BS, Belhekar AA (1996) J Catal 163:312
21. Tomishige K, Yamazaki O, Chen Y, Yokoyama K, Li X, Fujimoto K (1998) Catal Today 45:35
22. Tang S, Ji L, Lin J, Zeng HC, Tan KL, Li K (2000) J Catal 194:424
23. Zhang ZL, Verykios XE (1996) Appl Catal A: Gen 138:109
24. Slagtern A, Schuurman Y, Leclercq C, Verykios X, Mirodatos C (1997) J Catal 172:118
25. Choudary VR, Uphade BS, Mamman AS (1995) Catal Lett 32:387
26. Kroll VCH, Swaan HM, Mirodatos C (1996) J Catal 161:409
27. Tejuca LG, Fierro JLG (eds) (1992) Properties and applications of perovskite-type oxides. New York, p 271
28. Pietri E, Barrios A, Goldwasser MR, Pérez-Zurita MJ, Cubeiro ML, Goldwasser J, Leclercq L, Leclercq G, Gingembre L (2000) Stud Surf Sci Catal 30:3657
29. Pietri E, Barrios A, Gonzalez O, Goldwasser MR, Pérez-Zurita MJ, Cubeiro ML, Goldwasser J, Leclercq L, Leclercq G, Gingembre L (2001) Stud Surf Sci Catal 136:381
30. Lima SM, Assaf JM (2006) Catal Lett 108:63
31. Lima SM, Assaf JM, Peña MA, Fierro JLG (2006) Appl Catal A: Gen 311:94–104
32. de Lima SM, Assaf JM (2007) Química Nova 30–2:298
33. Monti DA, Baiker A (1983) J Catal 83:323; Malet P, Caballero A (1988) J Chem Soc Faraday Trans I 84:2369
34. Wagner CD, Davis LE, Zeller MV, Taylor JA, Raymond RH, Gale LH (1981) Surf Interface Anal 3:211
35. Garcia de la Cruz RM, Falcón H, Peña MA, Fierro JLG (2001) Appl Catal B 33:52
36. Requies J, Cabrero MA, Barrio VL, Güemez MB, Cambra JF, Arias PL, Perez-Alonso FJ, Ojeda M, Peña MA, Fierro JLG (2005) Appl Catal A: Gen 289:214–223
37. Peña MA, Fierro JLG (2001) Chem Rev 101:1981
38. Briggs D, Seah MP (1990) Practical surface analysis by Auger and and X-ray photoelectron spectroscopy, 2nd edn. Wiley, Chichester
39. Wagner CD, Davis LE, Zeller MV, Taylor JA, Raymond RH, Gale LH (1981) Surf Interface Anal 3:211
40. Rynkowski J, Samulkiewicz P, Ladavos AK, Pomonis PJ (2004) Appl Catal A: Gen 263:1–9
41. Trimm DL (1999) J Catal 49:3–10
42. Dias JAC, Assaf JM (2004) J Power Sources 137:264
43. Chesnokov VV, Zaikovskii VI, Buyanov RA, Molchanov VV, Plyasova LM (1995) Catal Today 24:265–267